Journal of
Materials Chemistry B

REVIEW

View Article Online
View Journal

Cite this: DOI: 10.1039/c7tb00891k

Carbon nanostructures in biology and medicine

Haiyun Liu,[a] Lina Zhang,[b] Mei Yan[ac] and Jinghua Yu *[ac]

Carbon nanostructures have unique physical, chemical, and electrical properties, which have attracted great interest from scientists. They are being successfully implemented in sensing, biomedical and biological related studies. This review selectively analyzes current advances in the field of carbon nanostructure bioapplications. A very detailed review is presented on how carbon nanomaterials are currently exploited for biosensing and biomedical applications. To begin with, properties of carbon nanostructures will be discussed, involving their unusual structure, extraordinary electronic properties and fascinating electron transport. The next major section deals with the exciting progress related to carbon materials in electrochemistry, including electrochemical sensing, biomedical and biological applications. We classify biosensors developed so far by their signal generation strategy and provide a comprehensive overview of them. In addition, we offer insights into how the carbon nanostructures are used in each sensor system and how they improve the sensing performance. Finally, prospects and further developments in this exciting field of carbon materials are also suggested. In particular, the biofunctionalization of carbon nanostructures for biomedical applications, biosensor development by using carbon nanomaterials, and the investigation of carbon nanomaterials for living cell studies are summarized in more detail. Future perspectives and possible challenges in this rapidly developing area are also discussed.

Received 31st March 2017,
Accepted 18th May 2017

DOI: 10.1039/c7tb00891k

rsc.li/materials-b

1 Introduction

Carbon nanostructures embrace a wide variety of carbon allotropes, with a large amount of shapes and sizes. This impressive development of new nanoforms of carbon has its origin in the discovery, thirty years ago,[1] of fullerenes by H. Kroto, R. Smalley and R. Curl who received in 1996 the Nobel Prize for this finding, thus opening the race for the discovery of other amazing carbon nanostructures. In the past decade carbon nanostructures have attracted major research interest as a viable alternative to electrical biosensors for applications in biosensing of a wide range of analytes. This is mostly due to the unique physical, chemical, optical, and electrical properties of carbon nanostructures. This has become possible *via* several of their inherent properties[2] with our established knowledge of molecular

[a] *Institute for Advanced Interdisciplinary Research, University of Jinan, Jinan Shandong, 250022, P. R. China. E-mail: ujn.yujh@gmail.com*
[b] *Shandong Provincial Key Laboratory of Preparation and Measurement of Building Materials, University of Jinan, Jinan, Shandong, 250022, P. R. China*
[c] *School of Chemistry and Chemical Engineering, University of Jinan, Jinan, Shandong, 250022, P. R. China*

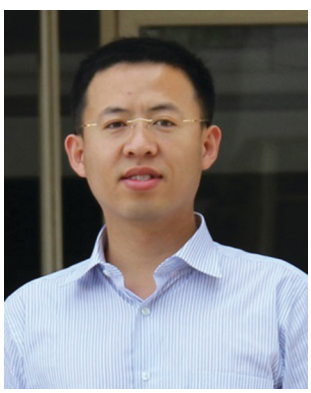

Haiyun Liu

Haiyun Liu obtained his PhD degree in chemical engineering and materials science from Shandong Normal University in 2014. He then joined the faculty at the University of Jinan, where currently he is a lecturer of chemistry. His current scientific interests are focused on nucleic acid DNA-based biosensors, bioimaging and biochemical analysis.

Lina Zhang

Lina Zhang received her BSc in applied chemistry from the University of Jinan in 2009, and obtained her PhD in civil engineering from the Hong Kong University of Science and Technology in 2014. Afterwards, she joined the faculty of the University of Jinan in the School of Material Science and Engineering as an Assistant Professor, with her research mainly focusing on surface functionalization of fibers and synthesis of nanomaterials.

and biomolecular recognition. This is due to ease of manipulation, biocompatibility as well as their performance as chemically robust platforms. Consequently, there has been a sustained interest in the use of carbon nanostructures for sensing applications.[3–6]

Carbon nanostructures exhibit huge diversity in structure, existing in allotropic forms, such as carbon dots (Cdots), carbon nanotubes (CNTs), and graphene as well as other less-explored carbon nanoforms such as graphene quantum dots (GQDs), nanodiamonds, carbon nanoonions, carbon nanohorns, *etc.* (Fig. 1). These materials can be classified according to the number of dimensions, which are not confined to the nanoscale range (<100 nm), *i.e.* nanoparticles, one-dimensional (1D) nanotubes and two-dimensional (2D) layered materials such as graphene.

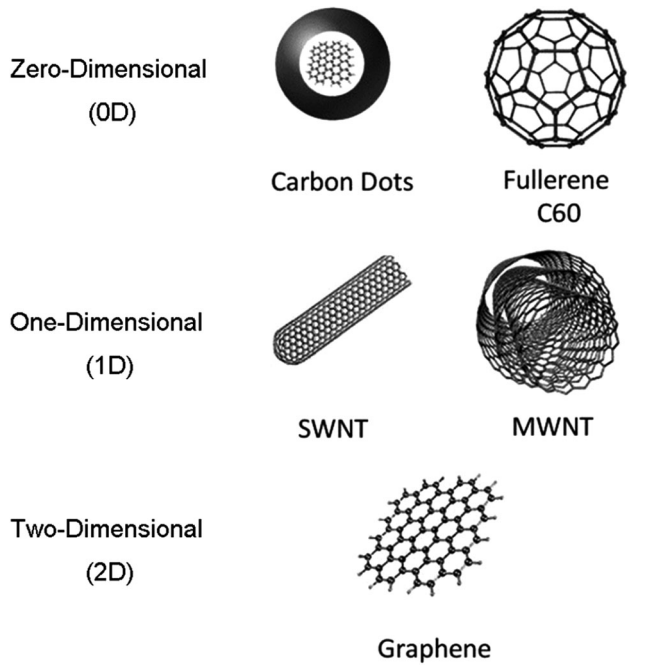

Fig. 1 Structures of carbon materials in biology and medicine.

2 Carbon nanostructures

2.1 Zero-dimensional carbon nanostructures

The first successful preparation of zero-dimensional (0D) fullerenes in macroscopic quantities by the evaporation and recondensation of graphite was reported in 1990.[7] 0D fullerenes are now readily available and exhibit exciting characteristics. For example, the delocalization of charges within the giant, spherical carbon framework together with the rigid, confined structure of the aromatic p-sphere offers unique opportunities for stabilizing charged entities. Above all, the small reorganization energies of fullerenes in charge transfer reactions have led to a notable breakthrough in synthetic electron donor–acceptor systems by providing accelerated charge separation and decelerated charge recombination.

The most recent addition to the 0D family of carbon nanostructures are Cdots, also referred to as GQDs. The earliest reported syntheses of Cdots were by the laser ablation of a carbon target[8] and from candle soot.[9] Today Cdots can be prepared by pyrolysis, hydrothermal and electrochemical treatments,[10] and microwave synthesis of a wide variety of carbon sources such as foodstuffs, biomass and waste materials.[10–12] These methods provide access to Cdots whose luminescence spans the visible spectrum.[13] In particular, Cdots are attractive for *in vivo* biosensing due to their biocompatibility.[3,14]

2.2 One-dimensional carbon nanostructures

The carbon nanotube, which can be considered a 1D allotrope of carbon, can be described as a ribbon of graphene being rolled into a cylindrical tube.[15–17] CNTs exhibit metallic, semimetallic and semiconducting properties which may be exploited for sensing applications.[3,5,18,19] These properties depend on the nature of the rolled graphene sheet, which dictates the chirality of the species. The synthesis of CNTs employs chemical vapour deposition of carbon in the presence of a transition metal catalyst.[20] In general, 1D single wall carbon nanotubes (SWCNTs) are considered as small strips of graphene-walled nanocylinders. CNTs are tubular structures of rolled-up sheets of graphene comprising SWCNTs and multi-wall carbon nanotube (MWCNT) species.

Mei Yan

Mei Yan received her BSc in applied chemistry from the University of Jinan in 1999, and obtained her PhD in 2005 from the Institute of Chemistry Chinese Academy of Sciences. She then joined the University of Jinan, as a professor, working on the synthesis and performance of advanced functional materials.

Jinghua Yu

Prof. Jinghua Yu received her BSc degree in applied chemistry from the Institute of Shandong Building Material and Industry in 1983, and obtained her PhD at the Lanzhou Institute of Chemical Physics in 2003. In 1983, she joined the University of Jinan and is undertaking research on bioanalysis, nanomaterials and microfluidic paper-on-chip devices.

2.3 Two-dimensional carbon nanostructures

The youngest representative of synthetic carbon allotropes is 2D graphene. Single graphene layers were first prepared successfully in 2004 by simple mechanical exfoliation of graphite using Scotch Tape.[21] Other fabrication strategies, in particular epitaxial growth and solubilization from bulk graphite, have been demonstrated and are paving the way to systematic experiments and technological applications.[22,23] Additionally, the symmetry of the experimentally measured conductance indicates high mobility for holes and electrons. An ideal monolayer of graphene has an optical transmittance of 97.7%. In summary, graphene should be a cost-effective and abundant source for transparent conductive electrode applications.

Graphene comprises a single layer of sp^2 carbon and as such can be considered the molecular parent of the sp^2 carbon nanostructures.[21] Graphene's ability to absorb light of all wavelengths coupled to its excellent electron transport properties has generated enormous interest.[24] Typically, graphene is prepared by mechanical and liquid phase exfoliation of graphite;[25,26] recently large scale preparation of graphene using surfactants has been reported.[27] In addition to pristine graphene, several surface treated forms such as photoluminescent graphene oxide (GO)[28] and reduced graphene oxide (RGO) have also been used for sensing applications.[29–31] GO is an oxygen-rich derivative of graphite created by strong oxidation, decorated with hydroxyl, epoxy, and carboxyl groups.[32] These oxygen-containing groups are distributed randomly on the basal planes and edges of the GO sheets. These functional groups provide a negative surface charge to the materials; owing to their polarity, they allow weak interactions like hydrogen bonding. The unmodified areas of the surface maintain their free p-electrons, making any p–p interactions feasible.[23,33] The structure, surface chemistry, charge, and hydrophilicity of GO may affect the conformational state and thus the catalytic activity of biomolecules.[34,35] RGO is usually considered as another kind of chemically derived graphene. The basal plane is similar to graphene except for defects by epoxides or hydroxides bound to the carbon atoms. For this reason, similar π-interactions will likely occur as shown with graphene, but there are additions of both hydrogen-bond donors and acceptor moieties from the epoxides, alcohols, ethers, carboxylic, and carboxylate oxygen-bearing moieties that can contribute an additional mode for interactions.[36]

3 Carbon nanostructures for electrochemical sensing

Carbon based nanostructures have emerged over the last few years as important agents for electrochemical sensors. In this review, developments in the last few years in the use of carbon nanostructure based electrochemical sensors for the detection of a range of analytes will be explored.

3.1 Carbon dot electrochemical sensors

Cdots have emerged as highly promising sensor materials and a number of reviews have been written describing their sensing applications.[6,38–41] In recent times, Yaqin Chai *et al.*[37] synthesized 2.3 nm diameter GQDs to fabricate an electrochemiluminescence (ECL) biosensor based on T7 exonuclease-assisted cyclic amplification and three-dimensional (3D) DNA-mediated silver enhancement for miRNA analysis. Aminated 3,4,9,10-perylenetetracarboxylic acid ($PTCA\text{-}NH_2$) was introduced to load GQDs through π–π stacking ($GQDs/PTCA\text{-}NH_2$), realizing solid-state GQD application. Fe_3O_4–Au core–shell nanocomposite ($Au@Fe_3O_4$) was adopted as a probe anchor to form a novel electrochemiluminescent signal tag of $GQDs/PTCA\text{-}NH_2/Au@Fe_3O_4$. Hairpin probe modified on the electrode was opened by helper DNA, followed by assembling of target to hybridize with the exposed stem of the helper DNA. T7 exonuclease was employed to digest the DNA/RNA duplex and trigger the target recycling without requiring a specific recognition site in the target sequence, realizing a series of RNA/DNA detections by changing the sequence of the complementary DNA. The ECL signal was further enhanced by silver nanoparticles (AgNPs)-based 3D DNA networks. After the two amplifications, the ECL signal of GQDs was extraordinarily increased and the prepared biosensor achieved a high sensitivity with a detection limit of 0.83 fM (Fig. 2). The ECL signal of GQDs could be improved by immobilizing them on the electrode due to the smaller distance. This sensing strategy can be expanded to explore an extensive range of DNA/RNA targets in real samples.

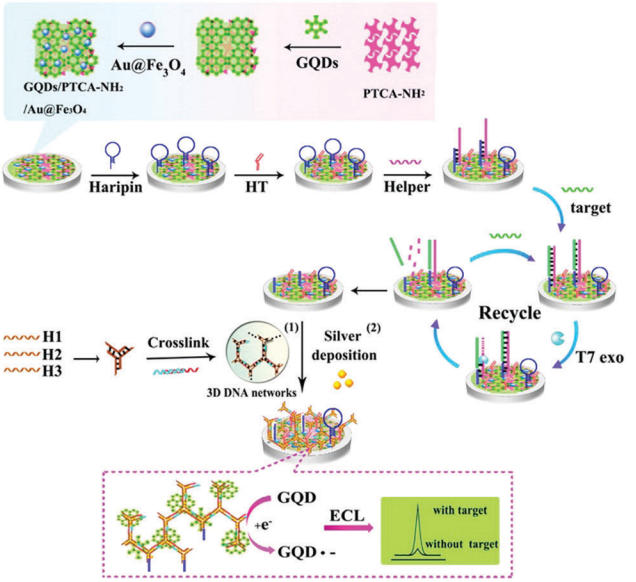

Fig. 2 ECL reaction mechanism for sensitive detection of miRNA.[37] Copyright (2015) American Chemical Society.

3.2 Carbon nanotube electrochemical sensors

Since their discovery, CNTs have attracted tremendous interest from the scientific community due to their unique physical and chemical properties.[43,44] The optical and electronic properties taken together with the structural properties make SWCNTs an ideal material for generating nanostructures suitable for an array of sensing applications.[42,45–47]

One example is the development of a SWCNT-based glucose sensor. A stable dispersion of SWCNTs bound to glucose

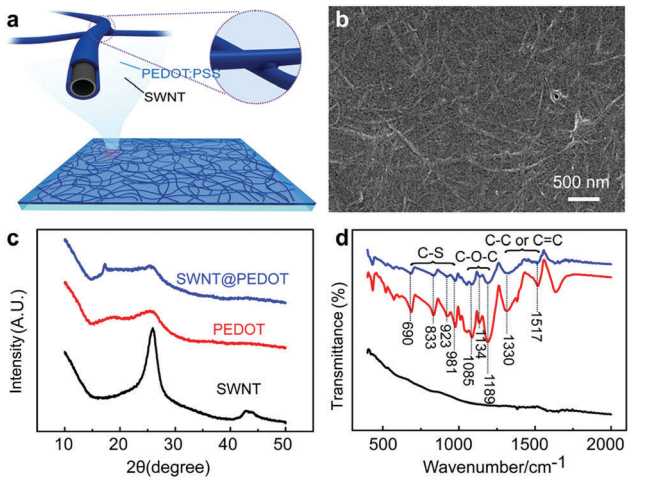

Fig. 3 Structural characteristics of hybrid film.[42] (a) Schematic illustration of the SWNTs@PEDOT/PDMS film. (b) SEM image of a SWNTs@PEDOT film. (c) XRD patterns. (d) IR spectra. Copyright (2017) American Chemical Society.

oxidase was employed. In this work small molecules, such as $Fe(CN)_6^{3-}$, can permeate the surface coating and bind non-covalently to the surface. This binding results in emission quenching. However, the H_2O_2, generated from the reaction of glucose with the enzyme, partially reduces the surface-bound $Fe(CN)_6^{3-}$ resulting in an increase in the emission.[48] This growth in emission then serves as a sensitive reporter of the H_2O_2 concentration.

Another example of a CNT-based stretchable and transparent electrochemical sensor was reported by Weihua Huang and co-workers in 2017.[42] The sensor involves binding SWNTs with conductive polymer to form composite films (Fig. 3). The films of nanometer thickness are produced by coating individual SWNTs with poly-(3,4-ethylenedioxythiophene) (PEDOT) followed by vacuum filtration. PEDOT coating effectively eliminates surface defects and provides favorable joint connections between individual SWNTs. The conductivity and electrochemical performances of composite films are greatly enhanced as compared to native CNT films. PEDOT protects the SWNT junctions from separation during stretching, which endows the sensor with high mechanical compliance and excellent electrochemical performance during big deformation. This work has constructed a CNT-based stretchable and transparent electrochemical sensor. It is proposed that further practical application may be broadened for wearable and *in vivo* implanted electrochemical sensing.

3.3 Graphene electrochemical sensors

To date, the use of graphene and related species has received the greatest interest for sensing. Graphene has come to the attention of the sensing community in recent years due to its unique properties and a number of reviews have been published detailing graphene and its sensing applications.[34,50–52] In particular, the properties of the 2D material have been employed in electrochemical based sensors. Graphene was used for electrical discrimination of circulating tumor cells and glucose as a highly conductive material.[53,54] There has even been electrochemical detection of different drugs by a graphene sensor.[55] Modified graphene/glassy carbon electrodes (GCEs) have demonstrated improved enhancement of sensitivity for single and multiple drug molecule detection. This is attributed to the increase of surface area, the conductivity of the nanoparticles and the added electroactivity arising due to the interaction of the molecules at the nanoparticle surface.

The electrocatalytical effect of GO on the oxidation of $Ru(bpy)_3^{2+}$ was observed at a GO-modified GCE in the absence of coreactants by Jun-jie Zhu (Fig. 4).[49] GO itself can act as the coreactant of $Ru(bpy)_3^{2+}$ ECL, which can be used to fabricate the ECL biosensor. Thiol group terminated ATP aptamer was immobilized on the GO film *via* DNA hybridization. When gold nanoparticles/graphene oxide (AuNPs/GO) nanocomposites were modified on the aptamer through the S–Au bond to form a sandwich-like structure, ECL resonance energy transfer could occur between $Ru(bpy)_3^{2+}$ and AuNPs/GO nanocomposites. After the ECL sensor was incubated in ATP solution, the AuNPs/GO nanocomposites were released from the electrode leading to an increased ECL signal. The proposed ECL aptasensor was fabricated and could be used in the sensitive and selective detection of ATP with a detection limit of 6.7 fM. This work revealed that GO and AuNPs are suitable materials for ECL resonance energy transfer research. Besides, Feng Li *et al.*[56] report a novel affinity-mediated homogeneous electrochemical aptasensor using a graphene modified GCE. The specific aptamer–target recognition is converted into an ultrasensitive electrochemical signal output with the aid of a novel T7 exonuclease-assisted target-analog recycling amplification strategy. This electrochemical aptasensor realizes the detection of biomolecules in a homogeneous solution without immobilization of any bioprobe on the electrode surface.

Another GO-based ECL sensor was fabricated based on a Hg^{2+} triggered signal switch coupled with an exonuclease I (Exo I)-stimulated target recycling amplification strategy for ultrasensitive determination of Hg^{2+} and MUC1 (Fig. 5).[57] The ECL intensity of *N*-(aminobutyl)-*N*-(ethylisoluminol) (ABEI)-functionalized silver nanoparticle-decorated graphene oxide nanocomposite (GO–AgNPs–ABEI) was initially enhanced by ferrocene labeled ssDNA Fc-S1 in the presence of H_2O_2. With the aid of aptamer,

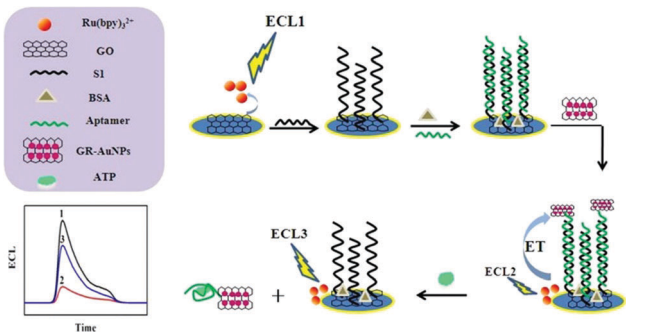

Fig. 4 The modification of a glassy carbon electrode (GCE) and the detection of ATP.[49] Copyright (2016) American Chemical Society.

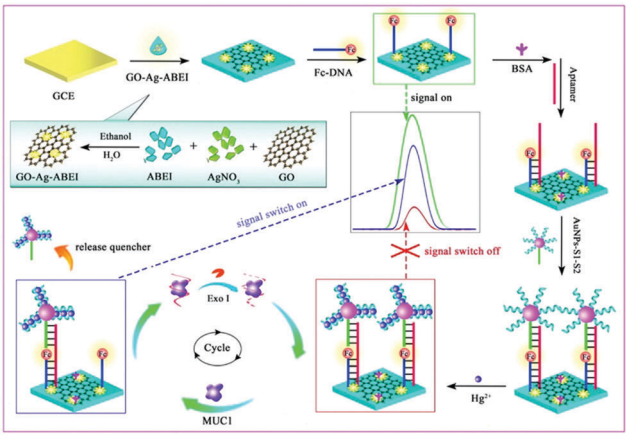

Fig. 5 Fabrication of the signal-switchable ECL aptasensor for Hg^{2+} and MUC1.[57] Copyright (2016) American Chemical Society.

assistant ssDNA S2 and full thymine bases, ssDNA S3 modified Au nanoparticles were immobilized on the sensing surface through a hybridization reaction. *Via* the strong and stable T–Hg^{2+}–T interaction, an abundance of Hg^{2+} was successfully captured on the AuNPs-S2-S3 and effectively inhibited the ECL reaction of ABEI. The signal switch "on" state was executed by utilizing MUC1 as an aptamer-specific target to bind aptamer, leading to a large decrease of the captured Hg^{2+}. Exo I was implemented to digest the bound aptamer, which resulted in the release of MUC1 for achieving target recycling with strong detectable ECL signal.

4 Carbon nanostructures for biomedicine

4.1 Carbon dots for biomedicine

Cdots have been used in recent times to detect a wide range of biomolecules and a range of drugs,[58,59] including hydrogen sulfide,[60,61] miRNA,[37] metal ions[12,58] and glucose.[62] The expression levels of these molecules are closely related to medical health. These have been detected in a variety of ways, including fluorescence quenching, fluorescence 'turn-off turn-on' methods, modified electrodes and target recognition.

One example of the use of a fluorescence sensor was demonstrated by Yunsheng Xia.[62] A simple and effective system which utilizes boronic acid functionalized Cdots was presented for the detection of glucose in the blood. The boronic acid functionalized particles were synthesized in a one-step "synthesis-modification integration strategy" using a phenyl boronic acid molecule as the sole precursor. The nanoparticles prepared possess a high volume of boronic acid groups at the Cdot surface, which act as glucose receptor sites. In the presence of glucose, cross-linking of Cdots occurs due to binding to receptor sites on different particles, which causes quenching of the Cdot emission (Fig. 6). This Cdot-based chemosensor needs no expensive enzymes and tedious surface modification procedures. This system has a limit of detection of 1.5 mM and selectivity against a range of interfering carbohydrates including sucrose,

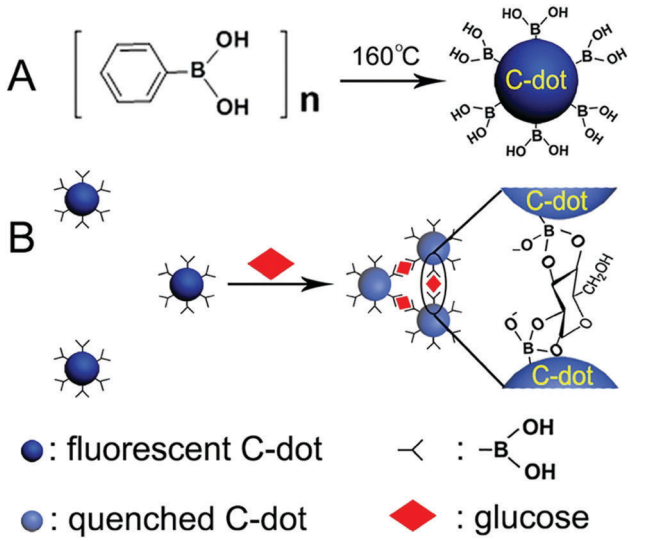

Fig. 6 (A) Formation of boronic acid functionalized carbon dots and (B) working principle for the sensing of glucose.[62] Copyright (2014) American Chemical Society.

fructose, lactose, and maltose and a range of amino acids and other biomolecules.

A further example of the application of Cdots for cellular sensing was reported by the Wu group,[60] who developed a fluorescence resonance energy transfer (FRET) ratiometric Cdot sensor for H_2S detection in aqueous media and live cells (Fig. 7). H_2S is related to diseases such as arterial and pulmonary hypertension and Alzheimer's disease. In this work Cdots serve as the energy donor and also the anchoring site for the probe. The sensor employed Cdots modified with an azo-naphthalimide probe that is reduced to an amino-naphthalimide in the presence of H_2S. In the absence of H_2S the blue emission of the Cdots is detected. The formation of the amino-naphthalimide generates a suitable energy acceptor of the Cdot emission, which yields green FRET emission at 526 nm. The appearance of the green emission was used to indicate the presence of H_2S in HeLa cells and murine aneuphloid fibrosarcoma cells.

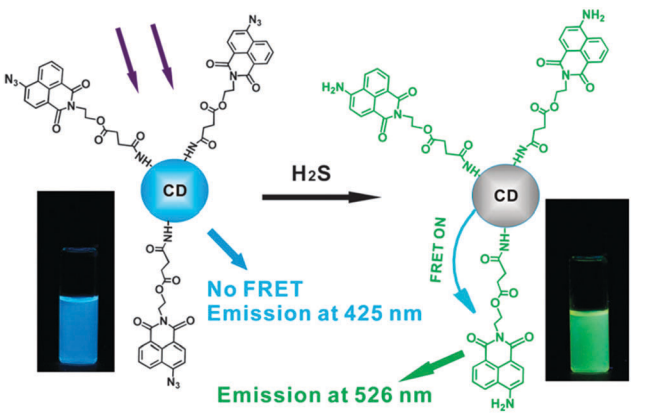

Fig. 7 Cdot-based sensor and its ratiometric detection of H_2S.[60] Copyright (2013) Royal Society of Chemistry.

Cdots are remarkable drug nanocarriers due to their promising optical and biocompatible capabilities. Yanli Zhao and colleagues developed tumor extracellular microenvironment-responsive drug nanocarrier based on cisplatin(IV) prodrug-loaded charge-convertible Cdots (Cdots–Pt(IV)@PEG-(PAH/DMMA)) for imaging-guided drug delivery.[63] An anionic polymer with dimethylmaleic acid (PEG-(PAH/DMMA)) on the fabricated Cdots–Pt(IV)@PEG-(PAH/DMMA) could undergo intriguing charge conversion to a cationic polymer in mildly acidic tumor extracellular microenvironment, leading to strong electrostatic repulsion and release of positive Cdots–Pt(IV). Positively charged nanocarrier displays high affinity to negatively charged cancer cell membrane. Cdots enhanced therapeutic effects as a smart drug nanocarrier *in vitro*. This provides a potential clinical application in cancer treatment. Shenqiang Zou and colleagues present a novel theranostic nanoplatform based on gadolinium-doped Cdots designed specifically for magnetic resonance imaging (MRI)-guided radiotherapy of tumors.[64] Gadolinium-doped Cdots enabled efficient passive tumor targeting as T1 contrast agents *in vivo*, exhibiting high longitudinal relaxation efficiency, long circulation time, radiosensitization enhancements and favorable biocompatibility. This work reported excellent T1 contrast agents and radiosensitizers, possessing great promise for MRI-guided radiotherapy of tumors. In particular, Gd-doped Cdots as enhancers of radiosensitivity highlight a novel avenue for overcoming resistance of solid tumors to radiotherapy.

4.2 Carbon nanotubes for biomedicine

The properties of CNTs have been exploited to develop a diverse range of biosensors.[43,44,65–67] CNTs can be modified with a biological sensing element, such as nucleic acids and peptides, and can also be modified with suitable groups capable of recognizing biomolecules, such as antibodies and enzymes, or monitoring bioprocesses. There have been a number of excellent reviews which have charted the progress of CNT biosensors.

A significant development was the immobilization of glucose oxidase onto the sidewalls of SWCNTs for the detection of glucose, first reported by Besteman *et al.*[68] The glucose oxidase-coated semiconducting SWCNTs were found to act as reversible pH sensors and showed an increase in conductance upon adding glucose, suggesting their use as a sensor for enzymatic activity. Another group employed sodium cholate stabilized semiconductor SWCNTs modified with boronic acid derivatives for glucose detection.[69] The sensors were found to allow glucose detection in a physiologically important range of 5 to 30 mM. Ahn *et al.* reported a label free approach capable of single protein–protein interaction detection using a SWCNT fluorescent sensor.[70] SWCNTs are embedded with a chitosan matrix bearing the chelator N_a,N_a-bis(carboxymethyl)-L-lysine. The matrix SWCNTs can bind to hexahistidine-tagged capture proteins. The capture protein is coupled to a Ni^{2+} chelate surrounding the SWCNTs. The intermolecular distance between Ni^{2+} ion and SWCNTs acts as a proximity quencher of the SWCNT fluorescence upon docking of the analyte proteins. This sensor exhibited a detection limit of 10 pM for an observation time of 600 s. A similar approach was followed for the detection of insulin by SWCNTs functionalised with insulin-binding aptamer as molecular recognition element.[71] Nanotherapeutics have been studied through a SWCNT dispersion agent, Evans blue (EB).[72] SWCNT based theranostic system has great promise in dual modalities imaging-guided PTT/PDT combined treatment of tumors. The applications of EB for SWCNT functionalization can be easily extended to other nanomaterials for improving their *in vivo* stability and circulation time.

CNTs labeled with aptamer and horseradish peroxidase (HRP) were used as a probe to amplify the impedimetric sensing of the aptamer–thrombin interaction (Fig. 8). The HRP-biocatalyzed oxidation of 3,3-diaminobenzidine (DAB) in the presence of H_2O_2 and the postelectropolymerization of insoluble precipitates produced on the electrode supports were used as a signal amplification route for the sensing process. Thrombin was sensed by aptamer 1 immobilized on a glassy carbon electrode. The MWCNT–aptamer 2-HRP probe was linked to the aptamer 1-thrombin complex through the thrombin–aptamer 2 interaction. The postelectropolymerization of biocatalyzed precipitates of DAB on the electrode greatly increased the electron-transfer resistance at the electrode–solution interface. Cyclic voltammetry and electrochemical impedance spectroscopy were employed to follow the stepwise fabrication of the aptasensor and impedimetric detection of thrombin. Thrombin concentration as low as 0.05 pM could be detected by this method.[73] In this work, the interaction between aptamer and thrombin can be greatly amplified by using MWCNT–apt2–HRP hybrids and postelectropolymerization of the precipitates produced by the enzymatically biocatalyzed reaction between HRP and DAB. It could be widely applied in the routine detection of proteins with high sensitivity and low detection limit.

A number of CNT biosensors for the detection of nucleic acids have also been reported (Table 1).[75–77] These sensors have been typically based on changes in a system's luminescence due to conformational changes in the DNA structure or recognition of complementary sequences. The fluorescence response of DNA modified SWCNTs has also been used for simultaneous detection of genotoxic analytes, including chemotherapeutic alkylating drugs, reactive oxygen species as well as single molecule

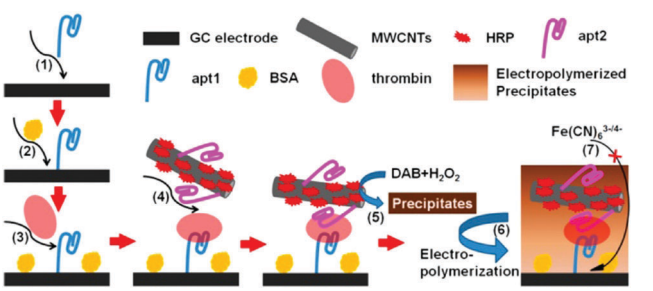

Fig. 8 The principle of the impedimetric aptasensor for thrombin detection:[73] (1) apt1 immobilization, (2) BSA blocking, (3) interaction between apt1 and thrombin, (4) signal amplification by MWCNT–apt2–HRP hybrids, (5) enzymatically biocatalyzed reaction between HPR and DAB, (6) post-electropolymerization of the precipitates, and (7) EIS measurements. Copyright (2015) American Chemical Society.

Table 1 Recent reports on carbon nanostructure-based biosensors for biomedicine

Analyte type	Carbon nanostructure	Target analytes	Limit of detection	Ref.
Protein	SWCNTs	Protective antigen toxin, anthrax	1 nM	21
Protein	SWCNTs	H63D mutation in the HFE gene	1 pM	89
Protein	SWCNTs	Immunoglobulin E (IgE)	250 pM	90
Protein	Graphene	Bovine serum albumin (BSA)	0.3 nM	91
Protein	RGO	Matrilysin	400 pM	92
Nucleic acid	SWCNTs	ssRNA	Not reported	93
Nucleic acid	SWCNTs	ssDNA	Single molecule	94
Nucleic acid	SWCNT	miRNA	1 aM	95
Nucleic acid	GO	ssDNA	2 nM	96
Nucleic acid	GO	ssDNA	100 fM	97
Nucleic acid	GO	ssDNA	2.4 nM	98
Nucleic acid	GO	ssDNA	10 fM	99
Nucleic acid	GO	ssDNA	Not reported	100
Nucleic acid	GO	ssDNA/miRNA	50 pM	101
Nucleic acid	GO	SNP	0.2 fM	102
Nucleic acid	GO	SNP	~1 nM	103

detection of H_2O_2.[78] The formation of a DNA coating at the surface results in strong SWCNT luminescence which is diminished upon DNA damage. The modulation of nanotube emission could then be correlated to the concentration of the DNA damaging agent using principal component analysis.

A simple and ultrasensitive miRNA electrochemical biosensor employing MWCNT–polyamidoamine (PAMAM) dendrimer and methylene blue redox indicator is reported (Fig. 9).[74] MiRNA expression is associated with cancer initiation, tumor stage, and tumor response to treatment. A glassy carbon (GC) electrode was modified with MWCNT–PAMAM, on which the oligonucleotide capture probes are immobilized. The MWCNT–PAMAM/GC electrode shows greatly enhanced signal to methylene blue (MB) reduction in contrast to bare GC electrode. The functionalization of MWCNTs with PAMAM maintains the electrochemical property of MWCNTs to MB reduction but minimizes the undesired adsorption of MB on the MWCNT surface. A detection limit of 0.5 fM was observed. This MWCNT–PAMAM-based biosensor exhibits good analytical properties.

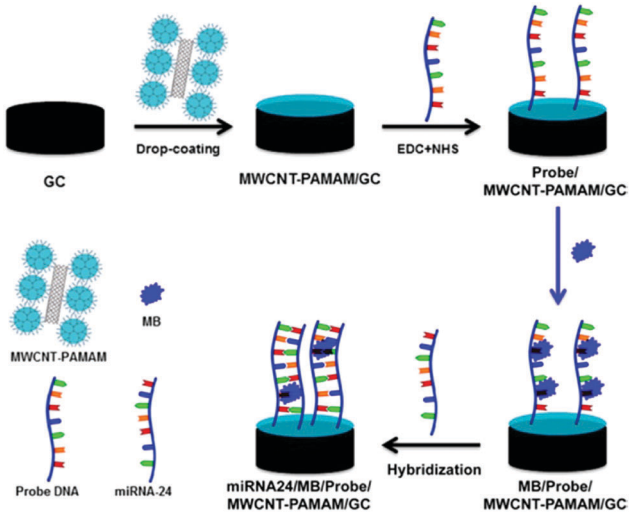

Fig. 9 MiRNA electrochemical biosensor based on MWCNT–PAMAM hybrids.[74] Copyright (2015) American Chemical Society.

4.3 Graphene for biomedicine

Recently a great number of graphene optical sensors have been developed (Table 1), and wide range of graphene sensors for drug detection have been reported. Graphene-containing sensors have been used to detect a wide range of biomolecules with great selectivity and sensitivity.[36,79–82] Xing *et al.* demonstrated the use of GO as a platform to detect target DNA through the use of a FRET based process. The same group used this approach to detect K^+. Fluorescein-labelled single stranded DNA was immobilized onto a sheet of GO where the emission is quenched. In the presence of the complementary strand of DNA binding occurs preventing the interaction of the fluorescently labelled sequence with the GO. The cationic conjugated polymer, PFP, is then added, which binds to the newly formed double stranded DNA, inducing FRET and giving a fluorescent signal. This detection is sensitive to single mismatches. In the presence of two or more mismatches the sequence remains at the GO surface. This is another nice example of a DNA sensor as its limit of detection was determined to be 40 pM with a fluorescence turn-on ratio of 7.60 in the presence of GO, as opposed to a ratio of 1.20 for traditional PFP systems. Graphene-based nanomaterials with different oxidation degrees were incorporated into Tetronic–tyramine hydrogels *via* enzymatic cross-linking.[83] The molecular oxidation of graphene in combination with amphiphilic Tetronic–tyramine significantly improved the water dispersibility of GO, resulting in a significant reinforcement of Tetronic–tyramine/GO composite hydrogels that can be used as an injectable biomaterial platform.

Choong *et al.*[84] developed a chemical-vapor-deposition-assisted method to synthesize 3D graphene foams (GFs), which were subsequently spin-coated with polymer to produce polymer-enriched 3D GFs with high conductivity and flexibility. This is a stepping stone toward future applications of polymer-enriched 3D GFs in the treatment of bone defects as well as other biomedical applications. Another study reported graphene platelet (GPL)-reinforced alumina (Al_2O_3) ceramic composites and the relationships between the loading of GPL and both mechanical properties and *in vitro* biocompatibility.[85] Mechanical properties of the Al_2O_3 matrix are significantly improved by adding GPLs.

The GPL/Al_2O_3 composites have comparable or more favorable biocompatibility. The excellent mechanical and biomedical properties of the GPL/Al_2O_3 composites may enable them to be applied to a wide range of engineering and biomedical applications.

Qingjie Ma *et al.* developed a fluorescent/photoacoustic imaging-guided photothermal therapy agent by seeding gold (Au) nanoparticles onto GO, which can further enhance photoconversion efficiency and improve photothermal tumor ablation effect of current nanomaterials.[86] The photothermal effect of GO/Au complex hybrid was found significantly elevated compared with GO alone. These studies further encourage applications of the hybrid nanocomposite for image-guided enhanced photothermal therapy in biomedical applications, especially in cancer theranostics. Dong-Eum Kim *et al.* have developed a facile fluorometric system for the detection of miRNA,[87] using rolling circle amplification, GO, and fluorescently labeled peptide nucleic acid. The isothermally amplified product containing miRNA sequences is less adsorbed onto the GO monolayer, attenuating the quenching of fluorescence by GO. Mandler *et al.*[88] described an electrochemically triggered drug delivery interface based on a flexible electrode consisting of thin gold films, deposited onto Kapton, coated with doxorubicin-loaded RGO thin films *via* electrophoretic deposition.

5 Carbon nanostructures for biological imaging

5.1 Carbon dots for biological imaging

Carbon dots, which can be seen as nanosized graphene or GO of <10 nm in size, bear much resemblance to GO in optical, in particular fluorescence, properties.[5] Carbon dots are considered as promising fluorescent tags. Carbon dots are highly photostable and resistive to photobleaching, as revealed by carbon dot labeled cell fluorescence imaging under prolonged illumination.[104] Furthermore, carbon dots do not contain any toxic elements for staining and imaging live organisms.[105] Besides, carbon dots are ultracompact fluorescent probes with extremely small footprints.[106]

Carbon dots have been widely applied for *in vitro* cell imaging. Sarkar *et al.* report labeling Ehrlich ascites carcinoma cells with fluorescent carbon dots and performing microscopic imaging (Fig. 10) of the labeled cells by collecting fluorescence of the carbon dots under both UV and blue light illuminations.[107] This approach can be used for milligram-scale synthesis of these water-soluble particles. The fluorescence property of these carbon dots is useful for cell-imaging. These carbon dots enter into cells without any further functionalization, and the fluorescence property of the carbon dots can be used to track their position in cells using a conventional fluorescence microscope.

Carbon dots can also be modified to have fluorescence responses to specific metal ions. Lin *et al.* report the successful preparation of truly FL excitation-dependent Cdots (also called full-color Cods, and abbreviated as F-Cods), which exhibit

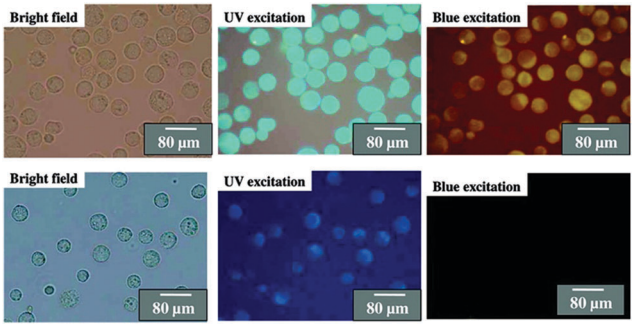

Fig. 10 Fluorescent Cdot-based labeling of Ehrlich ascites carcinoma cells.[107] The bottom row of images correspond to the control experiment where no Cdots were used. Copyright (2009) American Chemical Society.

unusually comparable emission intensity across nearly the entire visible spectrum with shifting of the excitation wavelength.[108] F-Cods could behave as multicolor bio-labeling reagents in cell imaging. Tian *et al.* report a conjugate consisting of both carbon dots and Cu^{2+}-chelating molecules that gradually loses its blue fluorescence at $\sim$500 nm with progressively increasing Cu^{2+} concentrations in the cytoplasm of cells.[109] When hybridized with a stably fluorescent CdSe/ZnS core/shell quantum dot nanostructure whose red fluorescence is inert to the Cu^{2+} cations, the nanohybrid can form a dual-emission ratiometric fluorescent sensor that changes color from blue (dominated by carbon dots) to red (dominated by CdSe quantum dots) upon addition of the Cu^{2+} ions.[110] Similar ratiometric intracellular fluorescent probes for Fe^{3+} [111] and O^{2-} [10] have been developed. Aptamer-conjugated carbon dots have also been reported to target and selectively label cancer cell lines while leaving normal healthy cells largely unstained.[112]

Carbon can not only be used for cell imaging, but also for live animal imaging. Sun *et al.* report the first *in vivo* fluorescence imaging in live mice using their photoluminescent carbon dots.[113] With subcutaneously injected carbon dots under the dorsal skin, bright fluorescence within the injected region can be clearly visualized as both green (525 nm) and red (620 nm) colors under 470 and 545 nm excitations, respectively. Migration of intradermally injected carbon dots to axillary lymph nodes can be observed after injection into the front extremity by tracking the fluorescence of the carbon dots. The results suggest that the carbon dots remain strongly fluorescent *in vivo*, which might offer great potential for imaging and related biomedical applications.

Besides regular fluorescence microscopic imaging, super-resolution imaging can also be performed on carbon dot-stained cells. Recently, Pompa *et al.*, for the first time, applied stimulated emission depletion microscopy to reveal the subdiffraction limit distribution of fluorescent carbon dots surrounding the cell nucleus with 60–80 nm feature size.[114] Since thus far carbon dots have not been found to be photoswitchable, other super-resolution microscopy techniques such as photoactivated localization microscopy[115] and stochastic optical reconstruction microscopy[116] have not been possible on carbon dot labeled samples, but the possibility of synthesizing photoswitchable

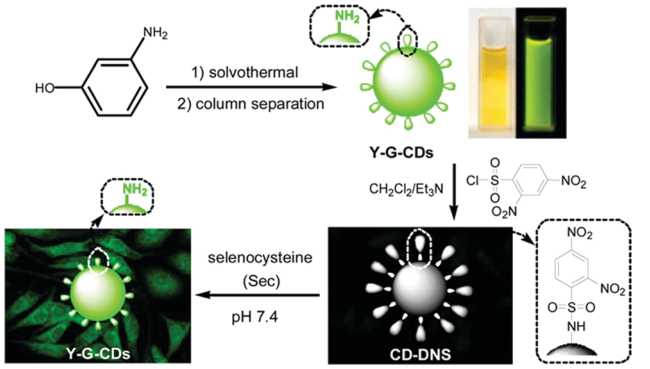

Fig. 11 Cdot-based imaging of selenol in living cells.[117] Copyright (2017) American Chemical Society.

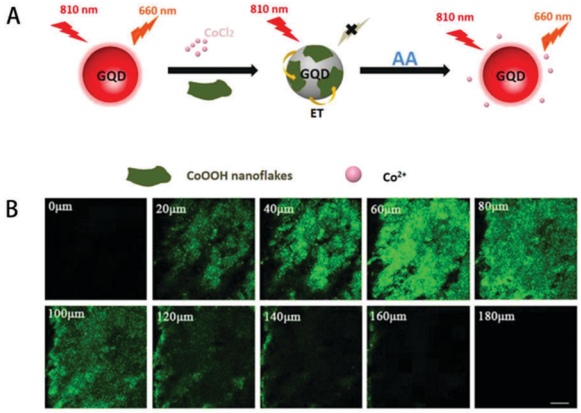

Fig. 12 The detection and cell imaging of ascorbic acid.[118] (A) Principle for ascorbic acid detection. (B) Fluorescence images of GQDs in tissue. Copyright (2017) American Chemical Society.

fluorescent carbon dots remains and could potentially make carbon dots more useful for biologists.

The excitation wavelength of reported Cdot-based probes is mainly located in the blue-light region, which hinders their applications for imaging studies in living cells. Li *et al.* developed a Cdot-based fluorescent turn-on probe for highly selective detection of selenol in living cells.[117] The highly photoluminescent carbon dots emit yellow-green fluorescence (Y-G-CDs). The surface of Y-G-CDs was then covalently functionalized with 2,4-dinitrobenzenesulfonyl chloride (DNS-Cl) to afford 2,4-dinitrobenzene-functionalized Cdots (CD-DNS) as a nanoprobe for selenol. Upon treating with selenocysteine, the DNS moiety of CD-DNS can be readily cleaved by selenolate through a nucleophilic substitution process, resulting in the formation of highly fluorescent Y-G-CDs and hence leads to a dramatic increase in fluorescence intensity. This is the first CD-based fluorescent probe for selenol that works under physiological conditions. This study shows that CD-DNS can function as a useful tool for fluorescence imaging of exogenous and endogenous selenol in living cells (Fig. 11).

Recently, near-infrared (NIR) GQDs have been developed for the detection of endogenous ascorbic acid in living systems.[118] GQDs possessed good two-photon fluorescence properties with a NIR emission at 660 nm upon exciting with 810 nm femtosecond pulses. The NIR GQDs exhibited lower fluorescence background in living system to afford improved fluorescence imaging resolution. This work was successfully used for two-photon imaging of endogenous ascorbic acid in living cells as well as deep tissue imaging (Fig. 12). The method can realize the direct detection of endogenous ascorbic acid in living cells, and could supply a novel platform for the analysis of biological targets *in vitro* and *in vivo*.

5.2 Carbon nanotubes for biological imaging

SWCNTs have great promise for use in biological imaging due to their excellent properties such as low cytotoxicity, high photostability, absence of quenching, and photobleaching in cells if functionalized properly.[119,120] Modified SWCNTs are commonly used in biological imaging.[72,121,122] Although SWCNTs covalently conjugated with organic fluorophores of shorter emission wavelengths had been imaged with confocal fluorescence microscopy in cells,[123] a groundbreaking piece of work demonstrating cell imaging by detecting the intrinsic fluorescence of SWCNTs was achieved for the first time by Weisman *et al.*, who incubated Pluronic surfactant stabilized SWCNTs with macrophages and successfully imaged the intracellular distribution of fluorescent SWCNTs that were phagocytosed into the cell cytoplasm during the incubation.[124] The intracellular distribution of internalized SWCNTs has been found as many bright, highly localized regions in the NIR-II fluorescence image, which are believed to be small phagosomes inside the cells. This finding provides a great opportunity for observing biological interactions between SWCNTs and biological systems through the direct detection of the intrinsic fluorescence of SWCNTs. The same group has shown that the intrinsic fluorescence of SWCNTs can be used to map the distribution of intravenously injected SWCNTs inside *ex vivo* rabbit liver tissues after euthanizing the rabbits and collecting the organs.[125]

The intrinsic nonlinear photoluminescence property of chemically functionalized multi-walled nanotubes MWNTs (f-MWNTs) is reported by Festy and Al-Jamal.[126] f-MWNTs are imaged by multiphoton photoluminescence and fluorescence lifetime imaging in fixed lung epithelial cancer cells and Kupffer cells *in vitro*, and in subcutaneously implanted solid tumors *in vivo*. Multiphoton imaging in the near-infrared excitation region provides sensitivity and resolution optimal for tracking f-MWNTs within intracellular compartments and facilitates tumor imaging and sentinel lymph node tracking *in vivo*. Wider applications include employing this technique in live imaging of f-MWNTs in biological milieu to facilitate image-guided drug delivery.

X-ray fluorescence could be supplied using contrast agents. CNTs can be filled with a wide range of inorganic materials, and thus can be used as 'contrast agents' if biologically absent elements are encapsulated. It has been shown that sealed SWCNTs filled with lead, barium and even krypton can be produced, and externally decorated with peptides to provide affinity for subcellular targets.[121] The agents are able to highlight specific organelles in multiplexed XRF mapping, and are a general and versatile tool for biological imaging.

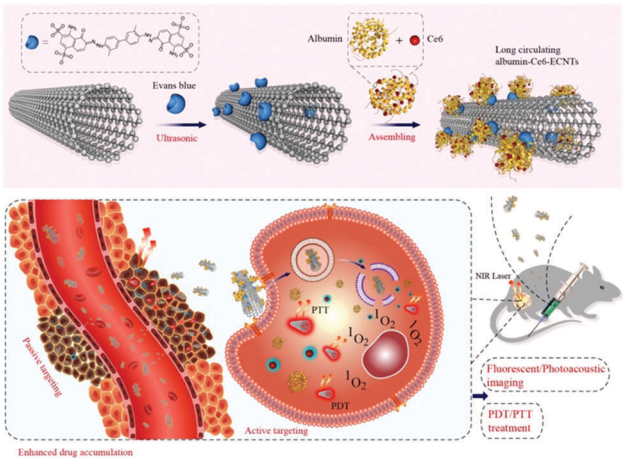

Fig. 13 Preparation and application of carbon nanotube-based delivery system.[72] Copyright (2016) Elsevier.

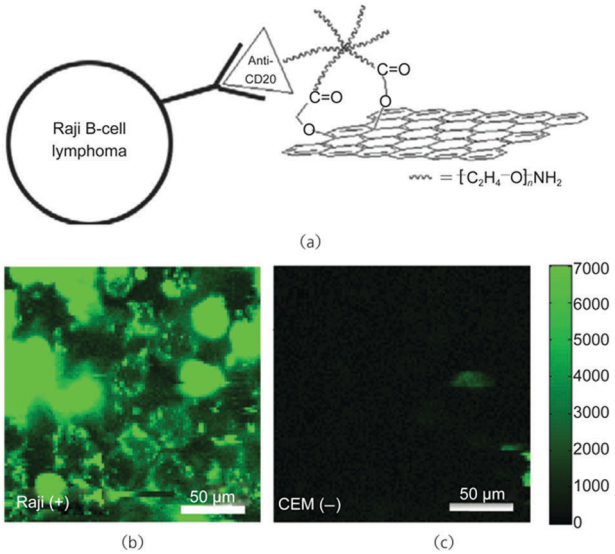

Fig. 14 Nano-graphene for targeted NIR living cells imaging. (a) The selective binding and cellular imaging of NGO–PEG conjugated with anti-CD20 antibody. (b) NIR fluorescence image of CD20 positive Raji B-cells treated with NGO–PEG–Rituxan conjugate. (c) NIR fluorescence image of CD20 negative CEM T-cells treated with NGO–PEG–Rituxan conjugate. Copyright (2008) Springer.

A novel long-circulating SWCNT-based therapeutic system was established to deliver Chlorin e6 (Ce6) by Lei Zhu *et al.* (Fig. 13).[72] The widely used photosensitizer has strong near-infrared fluorescence, for combined synergistic photodynamic therapy (PDT) and photothermal therapy (PTT). The SWCNT based theranostic system has great promise in dual modalities imaging-guided PTT/PDT combined treatment of tumors. Another example is a chromatographic separation method based on chirality-selective affinity between carbon nanotubes and a gel containing a mixture of surfactants.[122] In this work, chiral-angle selectivity and diameter selectivity are reported. Since the chirality of nanotubes is determined by the chiral angle and diameter, combining these independent selectivities leads to high-resolution single-chirality separation with milligram-scale throughput and high purity. Efficient vascular imaging of mice was used by separated single-chirality (9,4) nanotubes, which provide improved performance in biological imaging.

5.3 Graphene for biological imaging

Owing to the facile chemical synthesis of GO in solution phase, GO is the most common type of fluorescent graphene materials widely used for biomedical imaging.[127,128]

A few years ago, Dai *et al.* published the first paper on targeted cell imaging by employing the intrinsic NIR fluorescence of PEGylated GO (Fig. 14).[129] The starting material in this work, submicrometer-sized GO sheets, is broken down into much smaller pieces during PEGylation of the carboxyl functional groups that are abundant at the edges of the GO sheets, resulting in GO–PEG with an average lateral size of ~20 nm. The high selectivity of targeted fluorescence imaging using NGO–PEG reflects the distinct degrees of expression of CD20 on both cell lines and suggests the fluorescent NGO can be used for molecular phenotyping with sufficient sensitivity. Importantly, the intrinsic photoluminescence of GO is used for live cell imaging in the near-infrared with little background.

Logic gates in the imaging of different valent metal ions were applied in living cells. Zhang *et al.* have made a "smart" fluorescent probe with response to the concentration of Fe^{3+} ions by employing the selective fluorescence quenching properties of GO in the presence of Fe^{3+} ions.[130] GO can not only be used as a molecular imaging probe for certain membrane receptors, but can also afford intracellular functional imaging capability to sense the concentration of certain metal ions.

The graphene-based imaging method is also used for imaging other biomolecules in live cells. Li *et al.*[131] report for the first time the realization of a nanosensor tool that enables direct fluorescence activation imaging of Cyt *c* released from mitochondria in cell apoptosis. This strategy relies on spatially selective cytosolic delivery of a nanosensor constructed by assembly of a fluorophore-tagged DNA aptamer on PEGylated graphene nanosheets. The cytosolic release of Cyt *c* is able to dissociate the aptamer from graphene and trigger an activated fluorescence signal. For the first time, the spatially selective localization of an activatable nanocomplex sensor is developed for a "turn-on" fluorescence imaging mechanism of intracellular translocation events in living cells. The sensor was shown to exhibit large signal-to-background ratio *in vitro*.

The hybridization chain reaction-based *in situ* fluorescence imaging and detection of intracellular telomerase activity was developed by using GO.[132] The nanoflare probe consists of gold nanoparticles functionalized with a dense shell of nucleic acid sequences by Au–S bond formation. The nucleic acid sequence is composed of thiol-labeled sequence, telomerase primer sequence and FAM-terminated reporter sequence. The hybridization chain reaction is formed by two FAM-modified hairpin sequences that are adsorbed on GO. This work can sensitively detect telomerase activity in living cells, and distinguish normal cells from cancer cells (Fig. 15).

Recently, a folate receptor-targeted and cathepsin B-activatable nanoprobe was designed for background-free cancer imaging and

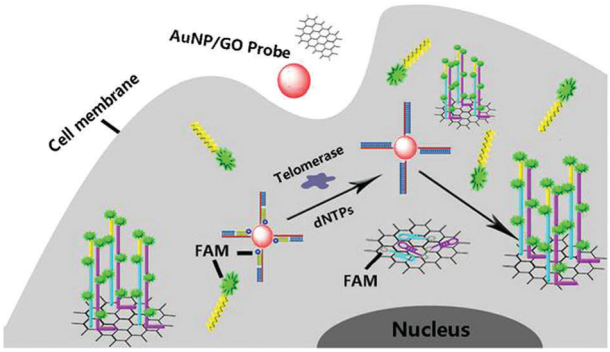

Fig. 15 *In situ* analysis and imaging of intracellular telomerase.[132] Copyright (2016) American Chemical Society.

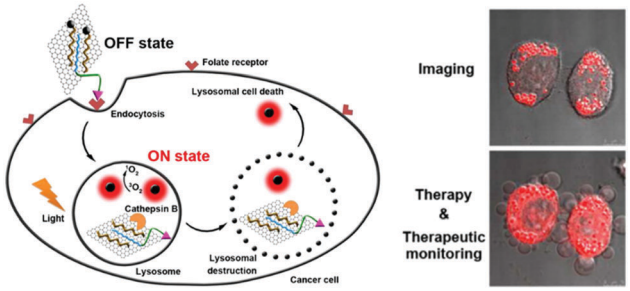

Fig. 16 Imaging and therapy of cathepsin B-activatable GO.[133] Copyright (2015) American Chemical Society.

selective therapy (Fig. 16).[133] The nanoprobe is prepared by noncovalently assembling phospholipid-poly(ethylene oxide) modified folate and photosensitizer-labeled peptide on the surface of GO. After selective uptake of the nanoprobe into lysosome of cancer cells *via* folate receptor-mediated endocytosis, the peptide can be cleaved to release the photosensitizer in the presence of cancer-associated cathepsin B, which leads to 18-fold fluorescence enhancement for cancer discrimination and specific detection of intracellular cathepsin B. Under irradiation, the released photosensitizer induces the formation of cytotoxic singlet oxygen for triggering photosensitive lysosomal cell death. After lysosomal destruction, the irradiated photosensitizer diffuses from lysosome into cytoplasm, which provides a visible method for *in situ* monitoring of therapeutic efficacy. This work provides a simple but powerful protocol with great potential in precise cancer imaging, therapy, and therapeutic monitoring.

6 Conclusions

Carbon nanostructures have emerged as an excellent sensing platform. These biosensors are notable for their high surface area, which allows many simultaneous detection events. Carbon nanostructures are truly distinguished from other nanomaterials by their diverse and robust intrinsic optical and electronic properties. The versatility of carbon nanostructures is demonstrated by the use of carbon dots, carbon nanotubes and graphene as either discrete molecular-like biosensors or assemblies and composites which can be integrated into devices. This continues to stimulate advances in the area of biosensing with an ever growing variety of systems being developed in recent years.

Carbon nanostructure-based electrochemical sensors and biomedical applications are considered in this review. The electroactivity of Cdots, CNTs and graphene has been extensively demonstrated for sensing, where their increased conductivity and surface area are readily exploited. This result suggests that further research is required to understand the contribution of these impurities to electrochemical carbon nanostructure biosensors. We have considered recent developments in the area of carbon nanostructure biosensors. We have described examples of carbon nanostructure fluorescence based sensing by Cdots, CNTs and GO materials. In particular the exciting developments include the use of carbon nanostructure platforms for cell imaging. Going forward, it is expected that carbon nanostructures will find greater application for *in vivo* sensing.

Going forward it is clear that realizing the potential of carbon nanostructures for routine sensing, and to see their widespread integration into sensing devices, necessitates the availability of sufficient quantities of pure and safe materials. This requires continued efforts in the areas of size-selective synthesis, purification and separation of carbon nanostructure species and consensus regarding the safety considerations. With progress on these fronts, the future of carbon nanostructure sensors is very bright indeed.

Acknowledgements

This work was financially supported by National Natural Science Foundation of China (21505052, 51502112, 21475052), Key Research and Development Program of Shandong Province, China (2016GGX102035), project funded by China Postdoctoral Science Foundation (2017M612169), and Science Foundation for Post Doctorate Research from the University of Jinan (XBH1509).

References

1 H. W. Kroto, J. R. Heath, S. C. O'Brien, R. F. Curl and R. E. Smalley, *Nature*, 1985, **318**, 162–163.
2 G. Konvalina and H. Haick, *Acc. Chem. Res.*, 2014, **47**, 66–76.
3 W. Yang, K. R. Ratinac, S. P. Ringer, P. Thordarson, J. J. Gooding and F. Braet, *Angew. Chem., Int. Ed.*, 2010, **49**, 2114–2138.
4 S. Zhu and G. Xu, *Nanoscale*, 2010, **2**, 2538–2549.
5 D. Jariwala, V. K. Sangwan, L. J. Lauhon, T. J. Marks and M. C. Hersam, *Chem. Soc. Rev.*, 2013, **42**, 2824–2860.
6 F. R. Baptista, S. A. Belhout, S. Giordani and S. J. Quinn, *Chem. Soc. Rev.*, 2015, **44**, 4433–4453.
7 W. Kratschmer, L. D. Lamb, K. Fostiropoulos and D. R. Huffman, *Nature*, 1990, **347**, 354–358.
8 Y.-P. Sun, B. Zhou, Y. Lin, W. Wang, K. A. S. Fernando, P. Pathak, M. J. Meziani, B. A. Harruff, X. Wang, H. Wang, P. G. Luo, H. Yang, M. E. Kose, B. Chen, L. M. Veca and S.-Y. Xie, *J. Am. Chem. Soc.*, 2006, **128**, 7756–7757.

9 H. Liu, T. Ye and C. Mao, *Angew. Chem., Int. Ed.*, 2007, **46**, 6473–6475.
10 X. Gao, C. Ding, A. Zhu and Y. Tian, *Anal. Chem.*, 2014, **86**, 7071–7078.
11 Z. Lin, W. Xue, H. Chen and J. M. Lin, *Anal. Chem.*, 2011, **83**, 8245–8251.
12 W. Wei, C. Xu, J. Ren, B. Xu and X. Qu, *Chem. Commun.*, 2012, **48**, 1284–1286.
13 S. N. Baker and G. A. Baker, *Angew. Chem., Int. Ed.*, 2010, **49**, 6726–6744.
14 C. Ding, A. Zhu and Y. Tian, *Acc. Chem. Res.*, 2014, **47**, 20–30.
15 S. Iijima, *Nature*, 1991, **354**, 56–58.
16 P. Avouris, Z. Chen and V. Perebeinos, *Nat. Nanotechnol.*, 2007, **2**, 605–615.
17 X. Zhang, G. Zhang, C. Zhao and X. Cheng, 4th International Conference on the Durability of Concrete Structures, 2014, pp. 212–218.
18 B. L. Allen, P. D. Kichambare and A. Star, *Adv. Mater.*, 2007, **19**, 1439–1451.
19 D. R. Kauffman and A. Star, *Angew. Chem., Int. Ed.*, 2008, **47**, 6550–6570.
20 D. S. Bethune, C. H. Klang, M. S. de Vries, G. Gorman, R. Savoy, J. Vazquez and R. Beyers, *Nature*, 1993, **363**, 605–607.
21 K. S. Novoselov, A. K. Geim, S. V. Morozov, D. Jiang, Y. Zhang, S. V. Dubonos, I. V. Grigorieva and A. A. Firsov, *Science*, 2004, **306**, 666–669.
22 G. Jing, Z. Ye, X. Lu and P. Hou, *Adv. Cem. Res.*, 2016, 1–8.
23 D. R. Dreyer, S. Park, C. W. Bielawski and R. S. Ruoff, *Chem. Soc. Rev.*, 2010, **39**, 228–240.
24 A. K. Geim and K. S. Novoselov, *Nat. Mater.*, 2007, **6**, 183–191.
25 M. J. Allen, V. C. Tung and R. B. Kaner, *Chem. Rev.*, 2010, **110**, 132–145.
26 J. N. Coleman, *Acc. Chem. Res.*, 2013, **46**, 14–22.
27 K. R. Paton, E. Varrla, C. Backes, R. J. Smith, U. Khan, A. O'Neill, C. Boland, M. Lotya, O. M. Istrate, P. King, T. Higgins, S. Barwich, P. May, P. Puczkarski, I. Ahmed, M. Moebius, H. Pettersson, E. Long, J. Coelho, S. E. O'Brien, E. K. McGuire, B. M. Sanchez, G. S. Duesberg, N. McEvoy, T. J. Pennycook, C. Downing, A. Crossley, V. Nicolosi and J. N. Coleman, *Nat. Mater.*, 2014, **13**, 624–630.
28 C. T. Chien, S. S. Li, W. J. Lai, Y. C. Yeh, H. A. Chen, I. S. Chen, L. C. Chen, K. H. Chen, T. Nemoto, S. Isoda, M. Chen, T. Fujita, G. Eda, H. Yamaguchi, M. Chhowalla and C. W. Chen, *Angew. Chem., Int. Ed.*, 2012, **51**, 6662–6666.
29 S. Eigler and A. Hirsch, *Angew. Chem., Int. Ed.*, 2014, **53**, 7720–7738.
30 V. Georgakilas, M. Otyepka, A. B. Bourlinos, V. Chandra, N. Kim, K. C. Kemp, P. Hobza, R. Zboril and K. S. Kim, *Chem. Rev.*, 2012, **112**, 6156–6214.
31 I. V. Pavlidis, M. Patila, U. T. Bornscheuer, D. Gournis and H. Stamatis, *Trends Biotechnol.*, 2014, **32**, 312–320.
32 A. Lerf, H. He, M. Forster and J. Klinowski, *J. Phys. Chem. B*, 1998, **102**, 4477–4482.
33 H. Y. Mao, S. Laurent, W. Chen, O. Akhavan, M. Imani, A. A. Ashkarran and M. Mahmoudi, *Chem. Rev.*, 2013, **113**, 3407–3424.
34 Y. Liu, X. Dong and P. Chen, *Chem. Soc. Rev.*, 2012, **41**, 2283–2307.
35 D. Chen, L. Tang and J. Li, *Chem. Soc. Rev.*, 2010, **39**, 3157–3180.
36 V. Georgakilas, J. N. Tiwari, K. C. Kemp, J. A. Perman, A. B. Bourlinos, K. S. Kim and R. Zboril, *Chem. Rev.*, 2016, **116**, 5464–5519.
37 P. Zhang, Y. Zhuo, Y. Chang, R. Yuan and Y. Chai, *Anal. Chem.*, 2015, **87**, 10385–10391.
38 M. Iranifam, *TrAC, Trends Anal. Chem.*, 2016, **80**, 387–415.
39 S. Ge, F. Lan, L. Liang, N. Ren, L. Li, H. Liu, M. Yan and J. Yu, *ACS Appl. Mater. Interfaces*, 2017, **9**, 6670–6678.
40 L. Li, Y. Zhang, L. Zhang, S. Ge, H. Liu, N. Ren, M. Yan and J. Yu, *Anal. Chem.*, 2016, **88**, 5369–5377.
41 L. Liang, F. Lan, S. Ge, J. Yu, N. Ren and M. Yan, *Anal. Chem.*, 2017, **89**, 3597–3605.
42 Z. H. Jin, Y. L. Liu, J. J. Chen, S. L. Cai, J. Q. Xu and W. H. Huang, *Anal. Chem.*, 2017, **89**, 2032–2038.
43 T.-T. Tran and A. Mulchandani, *TrAC, Trends Anal. Chem.*, 2016, **79**, 222–232.
44 S. Kumar, R. Rani, N. Dilbaghi, K. Tankeshwar and K. H. Kim, *Chem. Soc. Rev.*, 2017, **46**, 158–196.
45 Y. Zhang, Y. Wen, Y. Liu, D. Li and J. Li, *Electrochem. Commun.*, 2004, **6**, 1180–1184.
46 D. J. Zang, L. Ge, M. Yan, X. R. Song and J. H. Yu, *Chem. Commun.*, 2012, **48**, 4683–4685.
47 Y. H. Wang, L. Ge, P. P. Wang, M. Yan, J. H. Yu and S. G. Ge, *Chem. Commun.*, 2014, **50**, 1947–1949.
48 P. W. Barone, S. Baik, D. A. Heller and M. S. Strano, *Nat. Mater.*, 2005, **4**, 86–92.
49 Y.-P. Dong, Y. Zhou, J. Wang and J.-J. Zhu, *Anal. Chem.*, 2016, **88**, 5469–5475.
50 M. Pumera, A. Ambrosi, A. Bonanni, E. L. K. Chng and H. L. Poh, *TrAC, Trends Anal. Chem.*, 2010, **29**, 954–965.
51 Y. Liu, Y. Liu, H. Feng, Y. Wu, L. Joshi, X. Zeng and J. Li, *Biosens. Bioelectron.*, 2012, **35**, 63–68.
52 Y. Zhang, M. Su, L. Ge, S. Ge, J. Yu and X. Song, *Carbon*, 2013, **57**, 22–33.
53 S. I. Han and K. H. Han, *Anal. Chem.*, 2015, **87**, 10585–10592.
54 M. Wu, S. Meng, Q. Wang, W. Si, W. Huang and X. Dong, *ACS Appl. Mater. Interfaces*, 2015, **7**, 21089–21094.
55 A. Afkhami, H. Khoshsafar, H. Bagheri and T. Madrakian, *Anal. Chim. Acta*, 2014, **831**, 50–59.
56 L. Ge, W. Wang, X. Sun, T. Hou and F. Li, *Anal. Chem.*, 2016, **88**, 2212–2219.
57 X. Jiang, H. Wang, H. Wang, R. Yuan and Y. Chai, *Anal. Chem.*, 2016, **88**, 9243–9250.
58 Y. Song, C. Zhu, J. Song, H. Li, D. Du and Y. Lin, *ACS Appl. Mater. Interfaces*, 2017, **9**, 7399–7405.
59 V. Biju, *Chem. Soc. Rev.*, 2014, **43**, 744–764.

60 C. Yu, X. Li, F. Zeng, F. Zheng and S. Wu, *Chem. Commun.*, 2013, **49**, 403–405.
61 L. Li, Y. Zhang, F. Liu, M. Su, L. L. Liang, S. G. Ge and J. H. Yu, *Chem. Commun.*, 2015, **51**, 14030–14033.
62 P. Shen and Y. Xia, *Anal. Chem.*, 2014, **86**, 5323–5329.
63 T. Feng, X. Ai, G. An, P. Yang and Y. Zhao, *ACS Nano*, 2016, **10**, 4410–4420.
64 F. Du, L. Zhang, L. Zhang, M. Zhang, A. Gong, Y. Tan, J. Miao, Y. Gong, M. Sun, H. Ju, C. Wu and S. Zou, *Biomaterials*, 2017, **121**, 109–120.
65 J. Bartelmess, S. J. Quinn and S. Giordani, *Chem. Soc. Rev.*, 2014, **44**, 4672–4698.
66 S. G. Ge, L. Ge, M. Yan, X. R. Song, J. H. Yu and J. D. Huang, *Chem. Commun.*, 2012, **48**, 9397–9399.
67 H. Liu, L. Zhang, M. Li, M. Yan, M. Xue, Y. Zhang, M. Su, J. Yu and S. Ge, *RSC Adv.*, 2016, **6**, 26147–26154.
68 K. Besteman, J.-O. Lee, F. G. M. Wiertz, H. A. Heering and C. Dekker, *Nano Lett.*, 2003, **3**, 727–730.
69 K. Yum, J.-H. Ahn, T. P. McNicholas, P. W. Barone, B. Mu, J.-H. Kim, R. M. Jain and M. S. Strano, *ACS Nano*, 2012, **6**, 819–830.
70 J.-H. Ahn, J.-H. Kim, N. F. Reuel, P. W. Barone, A. A. Boghossian, J. Zhang, H. Yoon, A. C. Chang, A. J. Hilmer and M. S. Strano, *Nano Lett.*, 2011, **11**, 2743–2752.
71 T.-G. Cha, B. A. Baker, M. D. Sauffer, J. Salgado, D. Jaroch, J. L. Rickus, D. M. Porterfield and J. H. Choi, *ACS Nano*, 2011, **5**, 4236–4244.
72 L. Xie, G. Wang, H. Zhou, F. Zhang, Z. Guo, C. Liu, X. Zhang and L. Zhu, *Biomaterials*, 2016, **103**, 219–228.
73 J. Li, J. Wang, X. Guo, Q. Zheng, J. Peng, H. Tang and S. Yao, *Anal. Chem.*, 2015, **87**, 7610–7617.
74 F. Li, J. Peng, Q. Zheng, X. Guo, H. Tang and S. Yao, *Anal. Chem.*, 2015, **87**, 4806–4813.
75 D. A. Heller, E. S. Jeng, T. K. Yeung, B. M. Martinez, A. E. Moll, J. B. Gastala and M. S. Strano, *Science*, 2006, **311**, 508–511.
76 E. S. Jeng, J. D. Nelson, K. L. Prather and M. S. Strano, *Small*, 2010, **6**, 40–43.
77 R. Yang, J. Jin, Y. Chen, N. Shao, H. Kang, Z. Xiao, Z. Tang, Y. Wu, Z. Zhu and W. Tan, *J. Am. Chem. Soc.*, 2008, **130**, 8351–8358.
78 D. A. Heller, H. Jin, B. M. Martinez, D. Patel, B. M. Miller, T.-K. Yeung, P. V. Jena, C. Hobartner, T. Ha, S. K. Silverman and M. S. Strano, *Nat. Nanotechnol.*, 2009, **4**, 114–120.
79 Y. Huang, X. Dong, Y. Shi, C. M. Li, L. J. Li and P. Chen, *Nanoscale*, 2010, **2**, 1485–1488.
80 C. Cheng, S. Li, A. Thomas, N. A. Kotov and R. Haag, *Chem. Rev.*, 2017, **117**, 1826–1914.
81 S. Pattnaik, K. Swain and Z. Q. Lin, *J. Mater. Chem. B*, 2016, **4**, 7813–7831.
82 C. Ma, H. Liu, T. Tian, X. Song, J. Yu and M. Yan, *Biosens. Bioelectron.*, 2016, **83**, 15–18.
83 Y. Lee, J. W. Bae, T. T. Hoang Thi, K. M. Park and K. D. Park, *Chem. Commun.*, 2015, **51**, 8876–8879.
84 J. K. Wang, G. M. Xiong, M. Zhu, B. Ozyilmaz, A. H. Castro Neto, N. S. Tan and C. Choong, *ACS Appl. Mater. Interfaces*, 2015, **7**, 8275–8283.
85 J. Liu, Y. Yang, H. Hassanin, N. Jumbu, S. Deng, Q. Zuo and K. Jiang, *ACS Appl. Mater. Interfaces*, 2016, **8**, 2607–2616.
86 S. Gao, L. Zhang, G. Wang, K. Yang, M. Chen, R. Tian, Q. Ma and L. Zhu, *Biomaterials*, 2016, **79**, 36–45.
87 C. Hong, A. Baek, S. S. Hah, W. Jung and D. E. Kim, *Anal. Chem.*, 2016, **88**, 2999–3003.
88 L. He, S. Sarkar, A. Barras, R. Boukherroub, S. Szunerits and D. Mandler, *Chem. Commun.*, 2017, **53**, 4022–4025.
89 A. Star, E. Tu, J. Niemann, J.-C. P. Gabriel, C. S. Joiner and C. Valcke, *Proc. Natl. Acad. Sci. U. S. A.*, 2006, **103**, 921–926.
90 K. Maehashi, T. Katsura, K. Kerman, Y. Takamura, K. Matsumoto and E. Tamiya, *Anal. Chem.*, 2007, **79**, 782–787.
91 Y. Ohno, K. Maehashi, Y. Yamashiro and K. Matsumoto, *Nano Lett.*, 2009, **9**, 3318–3322.
92 H. Chen, P. Chen, J. Huang, R. Selegard, M. Platt, A. Palaniappan, D. Aili, A. I. Tok and B. Liedberg, *Anal. Chem.*, 2016, **88**, 2994–2998.
93 M. T. Martínez, Y.-C. Tseng, N. Ormategui, I. Loinaz, R. Eritja and J. Bokor, *Nano Lett.*, 2009, **9**, 530–536.
94 S. Sorgenfrei, C.-Y. Chiu, R. L. Gonzalez, Y.-J. Yu, P. Kim, C. Nuckolls and K. L. Shepard, *Nat. Nanotechnol.*, 2011, **6**, 126–132.
95 P. Ramnani, Y. Gao, M. Ozsoz and A. Mulchandani, *Anal. Chem.*, 2013, **85**, 8061–8064.
96 R. Stine, J. T. Robinson, P. E. Sheehan and C. R. Tamanaha, *Adv. Mater.*, 2010, **22**, 5297–5300.
97 B. Cai, S. Wang, L. Huang, Y. Ning, Z. Zhang and G.-J. Zhang, *ACS Nano*, 2014, **8**, 2632–2638.
98 Z. Yin, Q. He, X. Huang, J. Zhang, S. Wu, P. Chen, G. Lu, P. Chen, Q. Zhang, Q. Yan and H. Zhang, *Nanoscale*, 2012, **4**, 293–297.
99 C. Zheng, L. Huang, H. Zhang, Z. Sun, Z. Zhang and G.-J. Zhang, *ACS Appl. Mater. Interfaces*, 2015, **7**, 16953–16959.
100 Q. Zhao, Y. Zhou, Y. Li, W. Gu, Q. Zhang and J. Liu, *Anal. Chem.*, 2016, **88**, 1892–1899.
101 F. Li, J. Chao, Z. Li, S. Xing, S. Su, X. Li, S. Song, X. Zuo, C. Fan, B. Liu, W. Huang, L. Wang and L. Wang, *Anal. Chem.*, 2015, **87**, 3877–3883.
102 Y. Huang, H. Y. Yang and Y. Ai, *Anal. Chem.*, 2015, **87**, 9132–9136.
103 J. Huang, Z. Wang, J. K. Kim, X. Su and Z. Li, *Anal. Chem.*, 2015, **87**, 12254–12261.
104 Y. Fang, S. Guo, D. Li, C. Zhu, W. Ren, S. Dong and E. Wang, *ACS Nano*, 2012, **6**, 400–409.
105 S.-T. Yang, X. Wang, H. Wang, F. Lu, P. G. Luo, L. Cao, M. J. Meziani, J.-H. Liu, Y. Liu, M. Chen, Y. Huang and Y.-P. Sun, *J. Phys. Chem. C*, 2009, **113**, 18110–18114.
106 G. E. LeCroy, S. K. Sonkar, F. Yang, L. M. Veca, P. Wang, K. N. Tackett, 2nd, J. J. Yu, E. Vasile, H. Qian, Y. Liu, P. G. Luo and Y. P. Sun, *ACS Nano*, 2014, **8**, 4522–4529.
107 S. C. Ray, A. Saha, N. R. Jana and R. Sarkar, *J. Phys. Chem. C*, 2009, **113**, 18546–18551.
108 L. Pan, S. Sun, A. Zhang, K. Jiang, L. Zhang, C. Dong, Q. Huang, A. Wu and H. Lin, *Adv. Mater.*, 2015, **27**, 7782–7787.
109 Q. Qu, A. Zhu, X. Shao, G. Shi and Y. Tian, *Chem. Commun.*, 2012, **48**, 5473–5475.

110 A. Zhu, Q. Qu, X. Shao, B. Kong and Y. Tian, *Angew. Chem., Int. Ed.*, 2012, **51**, 7185–7189.
111 S. Zhu, Q. Meng, L. Wang, J. Zhang, Y. Song, H. Jin, K. Zhang, H. Sun, H. Wang and B. Yang, *Angew. Chem., Int. Ed.*, 2013, **52**, 3953–3957.
112 C. H. Lee, R. Rajendran, M. S. Jeong, H. Y. Ko, J. Y. Joo, S. Cho, Y. W. Chang and S. Kim, *Chem. Commun.*, 2013, **49**, 6543–6545.
113 S.-T. Yang, L. Cao, P. G. Luo, F. Lu, X. Wang, H. Wang, M. J. Meziani, Y. Liu, G. Qi and Y.-P. Sun, *J. Am. Chem. Soc.*, 2009, **131**, 11308–11309.
114 G. Lemenager, E. De Luca, Y. P. Sun and P. P. Pompa, *Nanoscale*, 2014, **6**, 8617–8623.
115 E. Betzig, G. H. Patterson, R. Sougrat, O. W. Lindwasser, S. Olenych, J. S. Bonifacino, M. W. Davidson, J. Lippincott-Schwartz and H. F. Hess, *Science*, 2006, **313**, 1642–1645.
116 M. J. Rust, M. Bates and X. Zhuang, *Nat. Methods*, 2006, **3**, 793–795.
117 Q. Wang, S. Zhang, Y. Zhong, X. F. Yang, Z. Li and H. Li, *Anal. Chem.*, 2017, **89**, 1734–1741.
118 L. Feng, Y.-X. Wu, D.-L. Zhang, X. Hu, J. Zhang, P. Wang, Z.-L. Song, X.-B. Zhang and W. Tan, *Anal. Chem.*, 2017, **89**, 4077–4084.
119 N. W. Kam, M. O'Connell, J. A. Wisdom and H. Dai, *Proc. Natl. Acad. Sci. U. S. A.*, 2005, **102**, 11600–11605.
120 J. T. Robinson, G. Hong, Y. Liang, B. Zhang, O. K. Yaghi and H. Dai, *J. Am. Chem. Soc.*, 2012, **134**, 10664–10669.
121 C. J. Serpell, R. N. Rutte, K. Geraki, E. Pach, M. Martincic, M. Kierkowicz, S. De Munari, K. Wals, R. Raj, B. Ballesteros, G. Tobias, D. C. Anthony and B. G. Davis, *Nat. Commun.*, 2016, **7**, 13118.
122 Y. Yomogida, T. Tanaka, M. Zhang, M. Yudasaka, X. Wei and H. Kataura, *Nat. Commun.*, 2016, **7**, 12056.
123 N. W. Shi Kam, T. C. Jessop, P. A. Wender and H. Dai, *J. Am. Chem. Soc.*, 2004, **126**, 6850–6851.
124 P. Cherukuri, S. M. Bachilo, S. H. Litovsky and R. B. Weisman, *J. Am. Chem. Soc.*, 2004, **126**, 15638–15639.
125 P. Cherukuri, C. J. Gannon, T. K. Leeuw, H. K. Schmidt, R. E. Smalley, S. A. Curley and R. B. Weisman, *Proc. Natl. Acad. Sci. U. S. A.*, 2006, **103**, 18882–18886.
126 N. Rubio, L. M. Hirvonen, E. Z. Chong, J. T. Wang, M. Bourgognon, H. Kafa, H. A. Hassan, W. T. Al-Jamal, D. McCarthy, C. Hogstrand, F. Festy and K. T. Al-Jamal, *Chem. Commun.*, 2015, **51**, 9366–9369.
127 L. Li, J. Feng, H. Liu, Q. Li, L. Tong and B. Tang, *Chem. Sci.*, 2016, **7**, 1940–1945.
128 H. Liu, T. Tian, D. Ji, N. Ren, S. Ge, M. Yan and J. Yu, *Biosens. Bioelectron.*, 2016, **85**, 909–914.
129 X. Sun, Z. Liu, K. Welsher, J. T. Robinson, A. Goodwin, S. Zaric and H. Dai, *Nano Res.*, 2008, **1**, 203–212.
130 Q. Mei, C. Jiang, G. Guan, K. Zhang, B. Liu, R. Liu and Z. Zhang, *Chem. Commun.*, 2012, **48**, 7468–7470.
131 T.-T. Chen, X. Tian, C.-L. Liu, J. Ge, X. Chu and Y. Li, *J. Am. Chem. Soc.*, 2015, **137**, 982–989.
132 M. Hong, L. Xu, Q. Xue, L. Li and B. Tang, *Anal. Chem.*, 2016, **88**, 12177–12182.
133 J. Tian, L. Ding, Q. Wang, Y. Hu, L. Jia, J.-S. Yu and H. Ju, *Anal. Chem.*, 2015, **87**, 3841–3848.

